THE JOURNAL OF BIOLOGICAL CHEMISTRY VOL. 286, NO. 10, pp. 8534–8544, March 11, 2011

Solution Structure of the Guanine Nucleotide-binding STAS Domain of SLC26-related SulP Protein Rv1739c from *Mycobacterium tuberculosis*[*] [S]

Received for publication, July 16, 2010, and in revised form, December 1, 2010 Published, JBC Papers in Press, December 29, 2010, DOI 10.1074/jbc.M110.165449

Alok K. Sharma[‡§¶], Liwen Ye[§¶‖], Christina E. Baer[**], Kumaran Shanmugasundaram[‡§¶], Tom Alber[**], Seth L. Alper[‡§¶‖1,2], and Alan C. Rigby[‡§¶1,3]

From the [‡]Divison of Molecular and Vascular Medicine, [‖]Renal Division, [§]Center for Vascular Biology Research, Beth Israel Deaconess Medical Center, and [¶]Department of Medicine, Harvard Medical School, Boston, Massachusetts 02215 and the [**]Department of Molecular and Cell Biology, University of California, Berkeley, California 94720

The structure and intrinsic activities of conserved STAS domains of the ubiquitous SulP/SLC26 anion transporter superfamily have until recently remained unknown. Here we report the heteronuclear, multidimensional NMR spectroscopy solution structure of the STAS domain from the SulP/SLC26 putative anion transporter Rv1739c of *Mycobacterium tuberculosis.* The 0.87-Å root mean square deviation structure revealed a four-stranded β-sheet with five interspersed α-helices, resembling the anti-σ factor antagonist fold. Rv1739c STAS was shown to be a guanine nucleotide-binding protein, as revealed by nucleotide-dependent quench of intrinsic STAS fluorescence and photoaffinity labeling. NMR chemical shift perturbation analysis partnered with *in silico* docking calculations identified solvent-exposed STAS residues involved in nucleotide binding. Rv1739c STAS was not an *in vitro* substrate of mycobacterial kinases or anti-σ factors. These results demonstrate that Rv1739c STAS binds guanine nucleotides at physiological concentrations and undergoes a ligand-induced conformational change but, unlike anti-σ factor antagonists, may not mediate signals via phosphorylation.

The *sulP*/*SLC26* gene superfamily of anion transporters is conserved throughout phylogeny (1–3). Mutations reported among the 11 human *SLC26* genes underlie autosomal recessive congenital chondrodysplasia (4), diarrhea (5), goiter (6), and deafness (6, 7). Engineered null mutations in mouse *Slc26* genes with human orthologs as yet unassociated with human disease have generated phenotypes of nephrolithiasis (8, 9), distal renal tubular acidosis (10), gastric achlorhydria (10, 11), and altered regulation of bicarbonate secretion by duodenum (12) and pancreatic duct (13, 14). In yeast, plants, and worms, the *sulp* gene products mediate transport of SO_4^{2-}, whereas in mammals the related *SLC26* gene products transport a wide range of monovalent anions in addition to divalent SO_4^{2-} and oxalate. Although *sulp* genes are present in genomes throughout the eubacteriae and archeae, indirect evidence of anion transport function by bacterial SulP polypeptides has to date been presented only for *Mycobacterium tuberculosis* Rv1739c (15), *Synechococcus* BicA (16, 17), and *Escherichia coli* YchM (18).

The majority of bacterial SulP proteins and all known eukaryotic SulP/SLC26 proteins carry a C-terminal cytoplasmic "sulfate transporter anti-σ factor antagonist" (STAS)[4] domain that shares distant sequence homology with bacterial anti-σ factor antagonist proteins (19, 20). Bacterial σ factors control specific transcriptional programs through activation of core RNA polymerase. All σ factors are negatively regulated by anti-σ factors. In *Bacillus subtilis*, σ F (σ^F) initiates and controls the sporulation program. The anti-σ factor for σ^F is SpoIIAB, a Ser/Thr kinase under the inhibitory control of the anti-σ antagonist SpoIIAA. ATP-liganded SpoII AB binds and inhibits σ^F. SpoIIAA activates σ^F through sequestration of SpoIIAB (ATP), which displaces σ^F from its complex with SpoIIAB. SpoIIAA phosphorylation (at Ser^{58}) by bound SpoIIAB leads to its dissociation from the ADP form of SpoIIAB. Phosphorylated SpoIIAA can then be dephosphorylated by phosphatase SpoIIE (summarized in Ref. 21). However, the GTP-binding and hydrolase activities of SpoIIAA (22) have unclear physiological functions, and no known relationship to either sporulation or the growth-promoting functions of the ribosome-associated GTPase, Obg (23).

The structure of SpoIIAA has been solved by heteronuclear NMR in solution (24), and x-ray crystallography (25) in phosphorylated and unphosphorylated forms, and in complex with SpoIIAB bound to either ADP or ATP (21). Published prelim-

* This work was supported by National Institutes of Health Grants R01 DK43495 (to S. L. A.), P30 DK34854 (Harvard Digestive Diseases Center to S. L. A.), and P01 AI68135 (TB Structural Genomics Consortium to T. A.).

[S] The on-line version of this article (available at http://www.jbc.org) contains supplemental "Methods," Table S1, and Figs. S1–S8.

The atomic coordinates and structure factors (code 2KLN) have been deposited in the Protein Data Bank, Research Collaboratory for Structural Bioinformatics, Rutgers University, New Brunswick, NJ (http://www.rcsb.org/).

[1] Both authors contributed equally to this work.

[2] To whom correspondence may be addressed: 99 Brookline Ave., RN-380F, Boston, MA 02215. Tel.: 617-667-2930; Fax: 617-667-8040; E-mail: salper@bidmc.harvard.edu.

[3] Present address: ImClone Systems, 450 East 29th St., New York, NY 10016. To whom correspondence may be addressed: 99 Brookline Ave., RN-231, Boston, MA 02215. Tel.: 617-667-0637; Fax: 617-667-2913; E-mail: arigby@bidmc.harvard.edu.

[4] The abbreviations used are: STAS, sulfate transporter and anti-σ factor antagonist; SLC26, solute carrier family 26; SulP, sulfate permease; HSQC, heteronuclear single quantum correlation; CSP, chemical shift perturbation; IVS, intrinsic variable sequence; aa, amino acid; GTPγS, guanosine 5′-3-*O*-(thio)triphosphate; GDPβS, guanosine 5′-*O*-2-(thio)diphosphate; PDB, Protein Data Bank; CFTR, cystic fibrosis transmembrane conductance regulator.

inary structures of additional STAS domain proteins include the NMR solution structure of *Thermotoga maritima* putative anti-σ antagonist TM1442 in phosphorylated and unphosphorylated states (26), the NMR and crystal structures of *T. maritima* putative anti-σ antagonist TM1081 (27), and the crystal structure of the putative stressosome component RsbS from *Moorella thermoacetica* (28). The SpoIIAA structure has been used to model the eukaryotic SLC26 STAS domain, including congenital chloride diarrhea missense mutations in the human SLC26A3 domain that result in subtle chemical shift changes as detected by ^{1}H-^{15}N two-dimensional HSQC NMR (29). However, the amino acid assignments of this structure have not been reported and, until recently, no other structural information had been released for STAS domains of SulP/SLC26 anion transporters.

We have overexpressed and purified the 560-aa putative SO_4^{2-} transporter Rv1739c from *M. tuberculosis*, comprising an N-terminal trans-membrane domain (aa 1–414) and a C-terminal cytoplasmic STAS domain (aa 442–560) (15). Previously, we reported the secondary structural features present in the C-terminal STAS domain using heteronuclear NMR spectroscopy (30). Here we report the three-dimensional NMR structure of the Rv1739c STAS domain (aa 437–560). Using intrinsic fluorescence quench data and ^{1}H-^{15}N chemical shift perturbation (CSP) experiments, we demonstrate that the monomeric STAS domain binds guanine nucleotides at physiological concentrations. The purified STAS domain is also associated with detectable GTPase activity. CSP analysis reveals that STAS binding of GDP elicits a more extensive conformational perturbation than does GTP. *In silico* docking calculations support these CSP data, suggesting that GDP binds preferentially, whereas GTP binding involves a subset of the GDP-interacting residues. The overexpressed Rv1739c STAS domain is not a phosphoprotein as isolated from *E. coli* or *Mycobacterium smegmatis*, and is not phosphorylated *in vitro* by recombinant Ser-Thr kinases or anti-σ factors of *M. tuberculosis*. While this work was in editorial review, reports appeared presenting crystal and solution structures of a centrally deleted core portion of the STAS domain from rat Slc26a5/prestin (31) and a crystal structure of the full-length STAS domain from *E. coli* SulP protein YchM (18).

EXPERIMENTAL PROCEDURES

Purification of Rv1739c STAS Domain—A polypeptide encompassing aa 437–560 of Rv1739c was overexpressed for study of the STAS domain, based on alignment with STAS domains from *E. coli* ychM and Sultr1.2, and with structurally characterized STAS domains from anti-σ factor antagonists of *B. subtilis*, *Bacillus sphericus*, and *T. maritima* 1442. For clarity, Rv1739c 437–560 are referred to as Rv1739c STAS aa 1–124 in this study. The Rv1739c STAS domain containing a C-terminal His_6 tag was overexpressed in the *E. coli* strain Tuner DE4pLacI (Novagen) as previously described (30). The protein purified from the nickel-nitrilotriacetic acid column was >96% pure as detected by Coomassie Blue staining of SDS-PAGE or PFO-PAGE gels. Subsequent gel filtration (Superdex 75 FPLC) yielded a homogeneous single peak eluting at a retention time that corresponds to monomeric STAS (~15 kDa), and is observed as a single band on overloaded SDS-PAGE (supplemental Fig. S1). Protein identity was confirmed by mass spectrometry. Unlabeled and uniformly ^{13}C/^{15}N- or ^{15}N-labeled STAS-His_6 NMR samples of 0.7–1.0 mM concentration in 50 mM sodium phosphate, 275 mM NaCl, pH 7.2, were prepared and subjected to NMR spectroscopy (supplemental "Methods" and Ref. 30). Rv1739c STAS expression in *M. smegmatis* is described under supplemental "Methods".

NMR Spectroscopy—NMR experiments were performed at 298 K on a Bruker Avance 600 MHz spectrometer equipped with a 5-mm triple resonance PFG (z axis) probe. All NMR data were acquired in gradient-selected, sensitivity-enhanced mode. NMR data were processed using NMRPipe/NMRDraw processing software (32), and analyzed using ANSIG (33). Protein backbone and side chain resonances of ^{1}H, ^{13}C, and ^{15}N were assigned using standard two-dimensional, three-dimensional, and triple resonance experiments (34–36) as detailed under supplemental "Methods".

Restraint Generation and Structure Determination of Rv1739c STAS Domain—A set of correlated NOE cross-peaks were generated by manual and automated NOE assignment using CYANA-2.1 (37) in two-dimensional [^{1}H,^{1}H]-NOESY (τ_m = 90, 120, and 150 ms), three-dimensional ^{15}N-resolved [^{1}H,^{1}H]-NOESY (τ_m = 120 ms), and ^{13}C-resolved [^{1}H,^{1}H]-NOESY (τ_m = 120 ms) spectra. Distance restraints were derived from NOE cross-peak intensities and from hydrogen bond measurements. Dihedral angles were determined using standard protocols (37–39) as detailed under supplemental "Methods". Three-dimensional structures were calculated with CYANA-2.1 using the torsion-angle dynamics protocol (37) (supplemental "Methods"). An ensemble of 30 structures selected for stereochemical quality assessment and the lowest Cyana target function was subjected to molecular dynamics simulation in explicit water for refinement using CNS (40).

Structure quality was assessed with PROCHECK-NMR (41). The 25 structures of the highest refinement represented the solution structure of Rv1739c STAS. Figures were generated with MOLMOL (42) and VMD (43), and sequences were aligned with ClustalW and LALIGN.

Heteronuclear NMR Investigation of Rv1739c STAS-Nucleotide Interaction—The Rv1739c STAS interaction with nucleotides was measured by collecting a series of two-dimensional ^{1}H-^{15}N HSQC experiments. Rv1739c STAS was titrated with increasing concentrations of nucleotides to a saturating concentration of 20 mM. CSP data were determined using weighted-average chemical shifts ($\Delta\delta_{weighted}$) for each amino acid residue; $\Delta\delta_{weighted} = [(\Delta^{1}H)^2 + (\Delta^{15}N/5)^2]^{1/2}$ (see supplemental "Methods").

In Silico Docking of STAS-Nucleotide Complexes—*In silico* docking calculations were carried out using AutoDock Vina (44). An exhaustive search was carried out to find and cluster the best docked poses of the GDP and GTP complexes with Rv1739c STAS. The average structure of the STAS domain was used as a starting target molecule for these docking studies (see supplemental "Methods").

Photoaffinity Labeling of Rv1739c STAS Domain—Rv1739c STAS was incubated with biotinylated azido-GTP in the presence or absence of 2 mM GTP, and briefly irradiated. An

aliquot of the terminated reaction was electrophoresed, blotted, developed, and visualized as detailed (supplemental "Methods").

Intrinsic Fluorescence Quench of Rv1739C STAS—Gel filtration-purified Rv1739c STAS in buffer A (25 mM Tris, 100 mM NaCl, pH 7.2) was centrifuged before use. Free acid forms of ATP, GTP, and GDP (Sigma), GTPγS, and GDPβS (Jena Biosciences) of the highest purity available were prepared as stock solutions in buffer A. Rv1739c STAS (12–20 μM; initial volume 200 μl) was preincubated in 48-well plates at 24 °C with nucleotides in the absence or presence of 1 mM added $MgCl_2$ (final volume: 217 μl). Steady-state intrinsic fluorescence intensity of RV1739c STAS was then recorded at λ_{em} 290–400 nm at 2-nm intervals with fixed $\lambda_{ex} = 280$ nm (SpectraMax M5, Molecular Devices, Sunnyvale, CA) in the presence of sequentially increasing nucleotide concentrations or titrated with buffer A alone. Rv1739c STAS fluorescence at each nucleotide concentration was corrected for dilution and for inner filter effect contributions of added nucleotide, as described (45). The effects of identical sequential increases in added nucleotide were assessed on the intrinsic fluorescence of a mixture of free tryptophan plus 3 molar eq of free tyrosine (the 1:3 Trp:Tyr molar ratio reflected in the native Rv1739c STAS amino acid sequence), with identical data acquisition parameters and instrument settings. The inner filter effect correction factor was determined as the ratio of fluorescence intensity of the Trp:Tyr solution in the absence of nucleotide to that in the presence of nucleotide at each emission wavelength. The inner filter effect correction factor was ≤2 at all nucleotide concentrations.

Inner filter effect-corrected, normalized fluorescence intensity data were plotted as a function of nucleotide concentration and fit (SigmaPlot, Systat) to a single site ligand-binding model,

$$F_0 - F = \frac{\Delta F_{max} \times [S]}{K_d + [S]} \quad \text{(Eq. 1)}$$

where $F_0 - F$ is the change in fluorescence intensity at 316 nm (λ_{max}) following the addition of nucleotides at concentration [S], ΔF_{max} is the maximum change in fluorescence intensity, and K_d is the STAS-nucleotide dissociation constant.

Assay of Nucleotidase Activity—Rv1739c STAS or human RhoA-GST (as a positive control) were mixed with [γ-^{32}P]GTP or [γ-^{32}P]ATP. Reactions were stopped with SDS, and fractionated by thin layer chromatography (TLC). Excised spots containing inorganic [^{32}P]phosphate were counted (Packard Tri-Carb 2200CA) in Ecoscint A (National Diagnostics, Atlanta, GA) with 97% efficiency (supplemental "Methods").

Protein Phosphorylation Assays—See supplemental "Methods" for kinase overexpression and purification. *In vitro* phosphotransfer assays were performed in reaction buffer (300 mM NaCl, 50 mM Tris, pH 8.0, 0.5 mM Tris(2-carboxyethyl) phosphine hydrochloride, 10% glycerol). Each reaction contained 15 μg of STAS Rv1739c substrate and 1.5 μg of Ser/Thr kinase or anti-σ factor kinase. Reactions were initiated by simultaneous addition of 1 μCi of [γ-^{32}P]ATP (800 Ci/mmol and 10 mCi/ml; MP Biomedicals), 50 μM ATP (Sigma), and 0.5 mM $MnCl_2$. Reactions proceeded for 30 min at room temperature, then subjected to SDS-PAGE and imaged as described (46).

TABLE 1
Structural statistics for Rv1739c STAS domain of *M. tuberculosis*
Statistics for the ensemble of 25 energy-minimized structures.

Restraints		
NOEs		
Total	1692	
Intraresidue ($\|i-j\| = 0$)	447	
Sequential ($\|i-j\| = 1$)	538	
Medium range ($1 < (\|i-j\|) \leq 4$)	396	
Long range ($\|i-j\|) > 4$)	311	
Hydrogen bonds	88	
Average distance restraints per residue	14.4	
Dihederal angles	Φ	φ
$^{13}C^{\alpha}$ secondary shifts based	67	67
Generated using Talos[a]	96	96
Structural quality		
Ramachandran map of residues 1–124	(in %)	
Most favored regions	66.2	
Additionally allowed regions	26.5	
Generously allowed regions	5.3	
Disallowed regions	1.9	
Average root mean square deviation from mean coordinates[b] (in Å)		
Backbone atoms (N, C^{α}, C′)	0.87 ± 0.17	
All heavy atoms	1.36 ± 0.24	
Restraint violation		
Upper distance (>0.5 Å)	~1.57	
Dihedral angle (>5°)	0	

[a] Dihedral angles generated using chemical shifts of $^{13}C^{\alpha}$, $^{13}C^{\beta}$, $^{1}H^{N}$, $^{1}H^{\alpha}$, $^{13}C'$.
[b] Root mean square deviation value determined for residue range 15–121.

RESULTS

NMR Spectroscopy of Rv1739c STAS Domain

The 124-aa Rv1739c STAS domain (Rv1739c aa 437–560) with a C-terminal His_6 tag (supplemental Fig. S1) was expressed and purified for NMR spectroscopy and biophysical studies. Supplemental Fig. S2 shows sequential $^{13}C^{\alpha}$, and $^{13}C^{\beta}$ assignments for the first α-helix (supplemental Fig. S2*A*) and third β-strand in Rv1739c STAS (supplemental Fig. S2*B*). The ^{1}H-^{15}N two-dimensional HSQC spectrum of the STAS domain (30) exhibited well dispersed resonances for nearly all backbone and side chain proton-nitrogen pairs (supplemental Fig. S2*C*), with previously reported ^{1}H-, ^{15}N-, and ^{13}C-chemical shifts (BMRB accession number 16052) (30). Xaa-Pro peptide bond conformations were predicted from chemical shift values of ^{15}N, $^{1}H^{N}$, $^{1}H^{\alpha}$, $^{13}C^{\alpha}$, $^{13}C^{\beta}$, and ^{13}CO resonances using PROMEGA (spin.niddk.nih.gov/bax/software) revealed a *trans*-configuration for each of the 5 Pro residues of Rv1739c STAS.

Distance and Dihedral Restraints of Rv1739c STAS Domain

NMR-derived experimental restraints used in determining the three-dimensional structure of Rv1739c STAS consisted of 1692 unique NOEs, 88 hydrogen bond restraints, and 163 (φ, ψ)-backbone angle restraints (Table 1). Sequential and medium range NOEs are summarized in Fig. 1. Of 311 long range NOEs assigned, 68 are from $^{1}H^{\alpha}$ and $^{1}H^{N}$ backbone-side chain interactions, 200 are from side chain-side chain interactions, and 43 represent backbone-backbone interactions. Hydrophobic and aromatic residues contribute 62 and 34% of the long range NOEs identified in Rv1739c STAS.

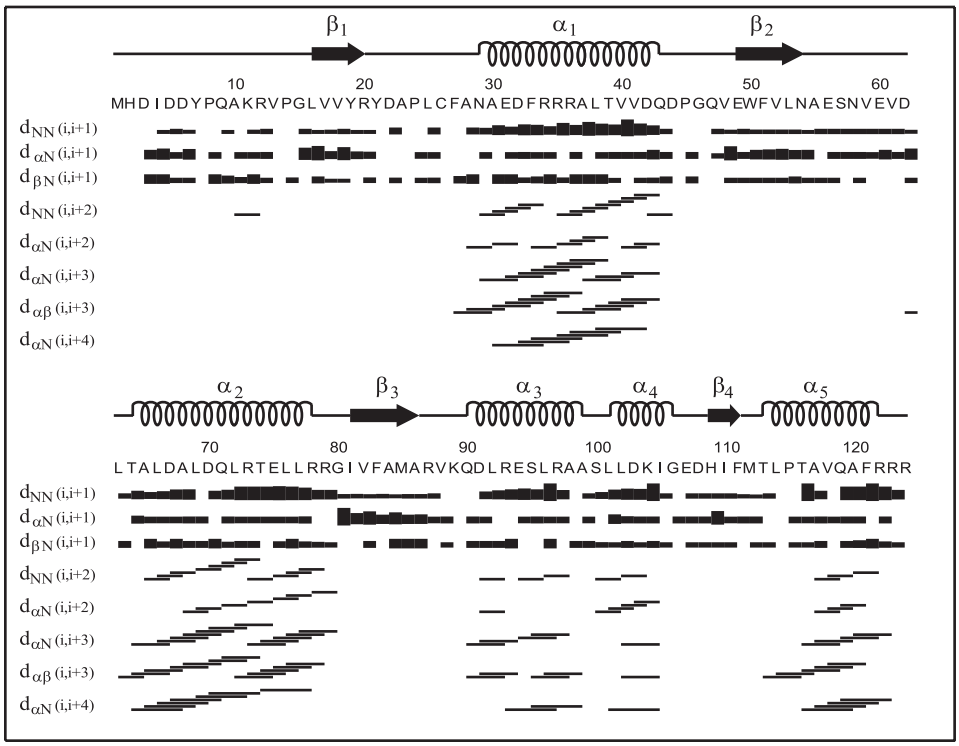

FIGURE 1. **Plot of sequential and medium range NOEs for Rv1739c STAS.** NOEs are assigned in three-dimensional ^{13}C- and ^{15}N-edited NOESY-HSQC, and two-dimensional ^{1}H-^{1}H NOESY spectra of Rv1739c STAS. *Bar thickness* is proportional to NOE intensity. α-Helices are depicted as *spirals*. β-Sheets are depicted as *arrows*.

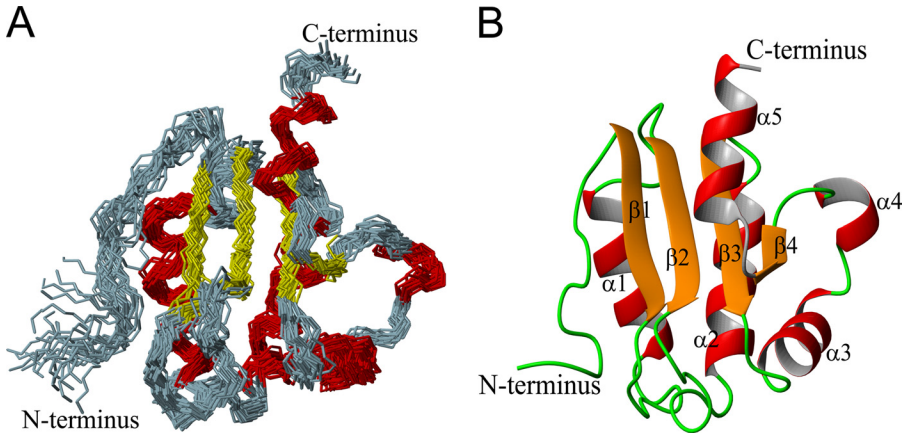

FIGURE 2. **Solution structure of Rv1739c STAS.** *A,* backbone representation (superimposed on N, C$^{\alpha}$, and C′ atoms) of an ensemble of the 25 lowest energy conformers of Rv1739c STAS. *B,* representative Rv1739c STAS conformer comprises a four-stranded β-sheet with five α-helices. The positions of the backbone and all heavy atoms exhibit root mean square deviation values of 0.87 ± 0.17 and 1.36 ± 0.24 Å, respectively, relative to the mean structure (Table 1). 98.1% of all residues occupy favorable or allowed regions within the Ramachandran map.

Three-dimensional Structure of Rv1739c STAS

Fig. 2*A* illustrates an ensemble of the 25 best NMR conformers of the Rv1739c STAS domain superimposed on their backbone N, C$^{\alpha}$, and C′ atoms. These structures were selected using standard structural criteria including: low target function, minimal upper distance NOE violations >0.5 Å, and absence of dihedral angle violations >5°. The low root mean square deviation values represented by the superimposed ensemble and the identification in allowed regions of the Ramachandran map of 98.1% of amino acid residues support the precision and stereochemical quality of the calculated structures (Table 1).

Fig. 2*B* presents the mean solution structure of Rv1739c STAS. The structure includes five well defined helices (α1, 30–42; α2, 65–77; α3, 91–99; α4, 102–105; and α5, 114–121), and four β-strands (β1, 16–19; β2, 50–53; β3, 82–86; and β4, 110–111) in a parallel orientation to form a β-sheet structure. Packing of helices α1 and α2 is stabilized by NOEs between adjacent regions within the fold. Supplemental Fig. S3*A* shows the calculated electrostatic potential surface of Rv1739c STAS. The net surface charge of −3 reflects 20 negatively charged and 17 positively charged surface residues that are distributed non-uniformly across the Rv1739c STAS surface.

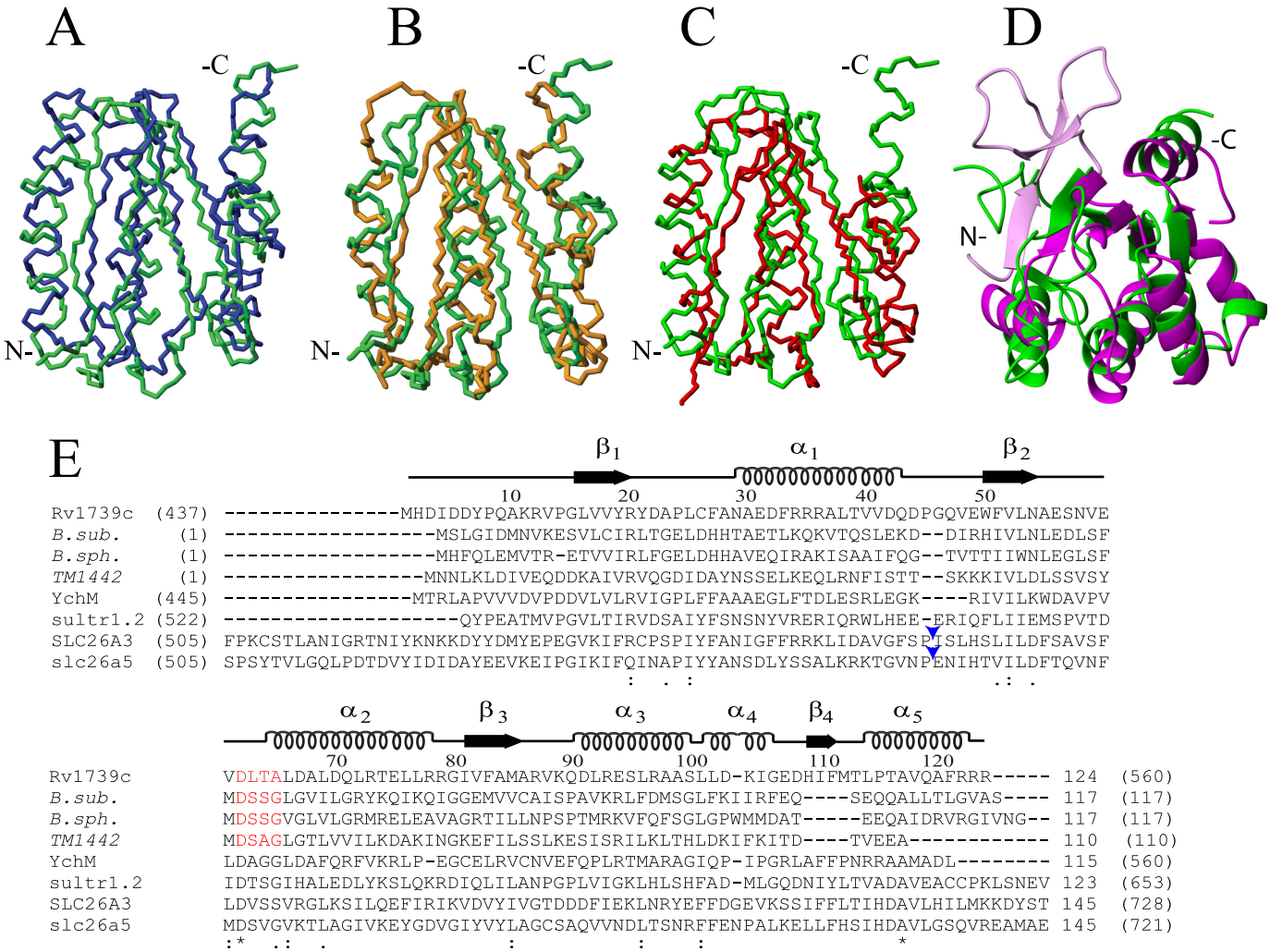

FIGURE 3. **Structural and sequence alignment of Rv1739c STAS domain.** *A–D,* average backbone structure of the Rv1739c STAS domain (*green*) aligned with: in *A,* crystal structure of non-phosphorylated SPOIIAA from *B. sphaericus* (*blue*, PDB code 1H4Z, root mean square deviation 3.6 Å); in *B,* solution NMR structure of *B. subtilis* SPOIIAA (*orange*, PDB code 1AUZ, root mean square deviation 3.9 Å); in *C,* solution NMR structure of *T. maritima* TM1442 (*red*, PDB 1SBO, root mean square deviation 3.3 Å); in *D,* overlay of a ribbon representation of Rv1739c STAS (*green*) with the crystal structure of an engineered core STAS domain from rat Slc26A5/prestin (*magenta*, PDB code 3LLO, root mean square deviation 3.3 Å). The region shown in *light magenta* comprises the N-terminal 15 aa of the prestin STAS (*light magenta*) extending beyond the Rv1739c STAS N-terminal residues. Backbone N, C^{α}, and C′ atoms were superposed onto secondary structured regions. (Overlays were obtained by superposition of backbone atoms as follows: in *A*, Rv1739c STAS domain residues 16–20, 30–42, 49–54, 65–77, 81–85, 91–98, and 114–120 were superposed on *B. sphaericus* SPOIIAA residues 12–16, 23–35, 44–49, 57–69, 76–80, 84–91, and 104–110. In *B*, STAS domain residues 16–20, 30–42, 49–54, 65–77, 81–85, and 91–97 were superposed on *B. subtilis* SPOIIAA residues 12–16, 25–37, 44–49, 60–72, 76–80, and 87–93. In *C*, STAS domain residues 16–20, 30–42, 50–54, 65–77, and 82–86 were superposed on TM1442 residues 14–18, 30–42, 46–50, 59–71, and 78–82. In *D*, Rv1739c STAS domain residues 16–20, 49–54, 65–77, 81–85, 91–98, and 110–111 were superposed on rat prestin STAS residues 536–540, 640–645, 655–667, 673–677, 681–688, and 702–703.) *E,* amino acid sequence alignment (ClustalW with manual adjustments) of Rv1739c STAS with STAS domains and structurally characterized anti-σ factor antagonists (*italicized*) from other organisms, including SpoIIAA from *B. subtilis* (*B. sub.*); SpoIIAA from *B. sphericus* (*B. sph.*), and *TM1442* (*T. maritima*). *Above* the aligned sequences are the tertiary structural elements and aa numbers of Rv1739c STAS. *Numbers in parentheses* are the aa residues encompassing each STAS domain or each (full-length) anti-σ factor antagonist. The conserved DSSG motif of *B. subtilis* SpoIIAA (*red*) and its phosphorylated residue Ser^{58} correspond to DLTA and Thr^{64} of Rv1739c STAS (*red*). The STAS domains from *E. coli* YchM and Sultr1.2 from *A. thaliana* are of lengths comparable with that of Rv1739c. The STAS domain of 764 aa human SLC26A3/DRA encompasses aa 505–728, and that of rat slc26a5/prestin encompasses aa 505–721. Both are shown with excision of the IVS region of ~75 aa between helix α_1 and strand β_2 (*blue arrowheads*, Rv1739c STAS-based nomenclature (28)). *Numbers* without parentheses at alignment C termini show lengths of the depicted sequences. In *parentheses* are the number of aa residues in each full-length polypeptide. *Asterisks under* the sequences mark positions of complete sequence conservation.

The structural order/rigidity of Rv1739c was evaluated using heteronuclear $\{^1H\}$-^{15}N NOE data obtained for 108 of 119 non-proline amino acids, and plotted as a function of amino acid sequence (supplemental "Methods" and Fig. S3*B*). The mean $\{^1H\}$-^{15}N NOE value for all residues was 0.79 ± 0.02, and was higher in more structured regions (0.84 ± 0.02) than in loop regions (0.71 ± 0.02). NOE values suggest the β2 (0.92 ± 0.02) and α4 (0.78 ± 0.05) regions as having higher and lower structural order/rigidity. The lower NOE value for the N-terminal 15 aa residues (0.55 ± 0.02) supports N-terminal fraying and conformational flexibility often associated with the presence of multiple prolines.

Structural Comparison of Rv1739c STAS with Other STAS Domains

Fig. 3, *A–D*, superimpose the backbone atoms of Rv1739c STAS with the crystal structure of non-phosphorylated *B. sphaericus* SpoIIAA, the NMR structure of *B. subtilis* SpoIIAA, the

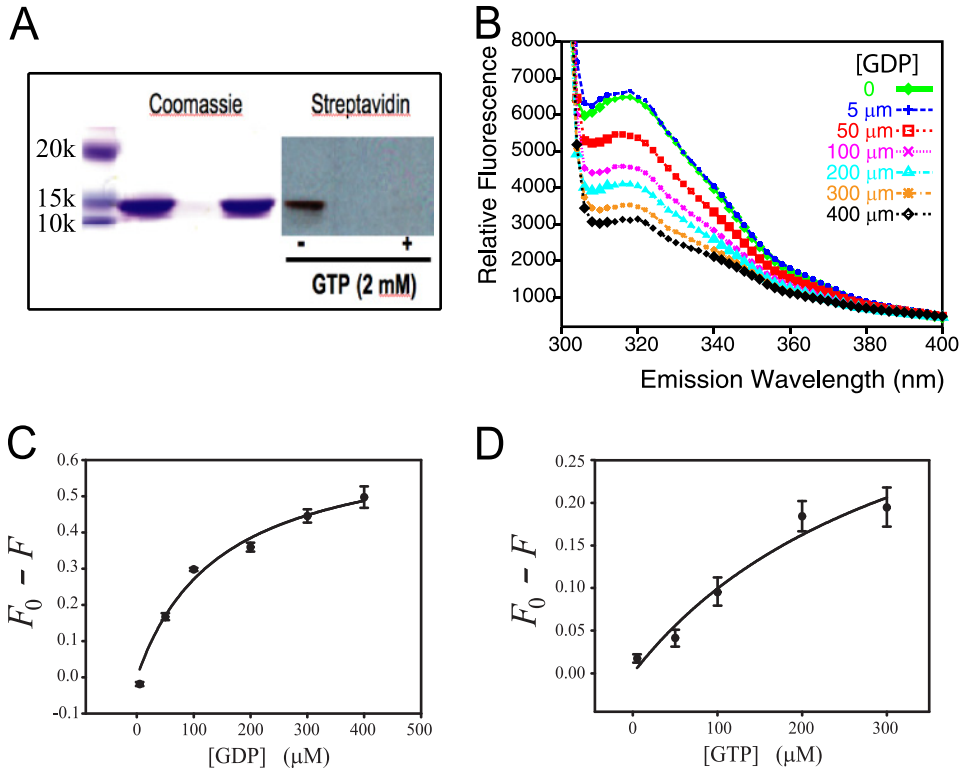

FIGURE 4. **Rv1739c STAS binds guanine nucleotides.** *A,* photoaffinity labeling of Rv1739c STAS with 8-N_3-GTP γ-biotinyl-LC-PEO-amine, in the absence and presence of 2 mM GTP. A representative of three similar experiments is shown. *B,* quench of intrinsic fluorescence of Rv1739c STAS (12–20 μM) by the indicated concentrations of GDP. *C,* concentration dependence for quench of the Rv1739c STAS peak intrinsic fluorescence by GDP ($K_{1/2}$ = 146 ± 38 μM; r^2 = 0.98). *D,* concentration dependence for quench of Rv1739c STAS peak fluorescence by GTP ($K_{1/2}$ = 347 ± 227 μM; r^2 = 0.96). λ_{ex} was 280 nm; λ_{em} was scanned between 300 and 400 nm. Values in *C* and *D* are mean ± S.E. ($n \geq 3$).

NMR structure of *T. maritima* TM1442, and the crystal structure of *Rattus norvegicus* Slc26a5/prestin. The structures are quite similar despite divergent primary sequence identities of <18%.

The overall tertiary fold of Rv1739c STAS resembles that of SpoIIAA from *B. sphaericus* and unphosphorylated SpoIIAA from *B. subtilis,* with one face of the central β-sheet juxtaposed to helices α1 and α2, and the other face exposed to the aqueous environment. The flexible structure of the N-terminal 14 aa residues of Rv1739c STAS contrasts with the structured N-terminal regions of SpoIIAA from *B. sphaericus* and *B. subtilis*. These include single β strands of 8 or 3 residues, respectively, packed in antiparallel orientation to the subsequent β strands arrayed in parallel, which together form a central β sheet. Helices α1 and α2 of Rv1739c STAS and *B. subtilis* SpoIIAA are similar in length, but shorter than the corresponding helices in *B. sphaericus* SpoIIAA. Helix α4 of Rv1739c STAS is oriented away from the protein core as in *B. sphaericus*, but closely packed to the main fold in *B. subtilis* and TM1442. Rv1739c STAS helix α3 extends parallel to the central β-sheet, in contrast to a perpendicular orientation of α3 in *B. subtilis* SpoIIAA. β1 and β2 strands of Rv1739c STAS and TM1442 are of similar length, but shorter than those of SpoIIAA. The β3-strands in Rv1739c (aa 80–86) and *B. sphaericus* SpoIIAA are similar in length. However, this region is shorter in length in TM1442 and unstructured in *B. subtilis* SpoIIAA.

The topological fold of Rv1739c STAS closely resembles that of the rat prestin construct truncated at its C terminus and devoid of its "intervening sequence" (IVS) region aa 564–636. A notable exception to this similarity is the N-terminal 15-aa extension present in prestin STAS, which includes a "β1 strand" at its extreme N terminus and a "β0 strand" in the immediately juxtaposed loop (31). Structural comparison among SulP/SLC26 polypeptides reveals that the presence of a common C-terminal β4 strand (aa 110–111 of Rv1739c STAS) is often absent from anti-σ factor antagonist structures. In addition, whereas helices α1 and α2 of anti-σ factor antagonists are arrayed in parallel orientation, the corresponding α1 and α2 helices of SulP/SLC26 STAS domains are oriented along divergent axes.

The conserved ^{56}DSSG motif of SpoIIAA constitutes a canonical phosphorylation site at Ser^{58} (Fig. 3*E*, in *red*). Sequence alignment suggests that Thr^{64} of Rv1739c, ^{62}DLTA (also in *red*), provides a homologous phosphorylation site of Rv1739c. Superimposed tertiary structures further support the alignment of Ser^{58} of SPOIIAA (PDB code 1AUZ) with the partially surface exposed Thr^{64} of Rv1739c STAS (PDB code 2KLN). These phosphorylation motifs in both SpoIIAA and Rv1739c are bracketed by hydrophobic residues. In addition to Thr^{64}, many conserved residues of Rv1739c STAS reside within a localized patch comprising the β2-α2 region (Fig. 3*E*).

Guanine Nucleotide Binding by Rv1739c STAS

The reported nucleotide binding properties of the anti-σ factor antagonist SpoIIAA (22) and the STAS domain of the blue light receptor YtvA from *B. subtilis* (47) prompted us to evaluate the nucleotide binding potential of Rv1739c STAS.

TABLE 2
Binding affinities of nucleotide-Rv1739c STAS interaction
$K_{½}$ values from fit of Rv1739c STAS fluorescence intensity quench by the indicated nucleotides at λ_{em} 316 nm.

Nucleotide	$K_{½}$ ± S.E.	r^2
	μM	
GTP	347 ± 227	0.96
GTPγS	326 ± 131	0.98
GTP + 1 mM $MgCl^2$	727 ± 251	0.99
GDP	146 ± 38	0.98
GDPβS	152 ± 53	0.98
GDP + 1 mM $MgCl_2$	587 ± 337	0.97
ATP	756 ± 232	0.94

As illustrated in Fig. 4*A*, Rv1739c STAS was photolabeled by a γ-biotinylated derivative of 8-N_3-GTP, and this photolabeling was prevented in the presence of excess unlabeled GTP. The presence of a unique Trp residue, Trp^{50} (aa 486 of Rv1739c holoprotein), in Rv1739c STAS and Tyr residues at STAS positions 7, 19, and 21 (Fig. 3*E* and supplemental Fig. S4*A*) allowed assessment of nucleotide binding using intrinsic fluorescence quench methods.

Rv1739c STAS fluorescence emission λ_{max} was observed at 316 nm. Fig. 4*B* illustrates the gradual quench of intrinsic STAS fluorescence with progressively increasing concentrations of GDP. Supplemental Fig. S4 shows comparable quench by increasing concentrations of GTP, of non-hydrolyzable guanine nucleotides, and ATP. The observed quench isotherms are compatible with a single nucleotide binding site with dissociation constants ($K_{½}$, in μM) of 146 ± 38 for GDP, 347 ± 227 for GTP (Fig. 4, *C* and *D*), 152 ± 53 for GDPβS (supplemental Fig. S4, *E* and *F*), and 326 ± 131 for GTPγS (supplemental Fig. S4, *C* and *D* and Table 2). $K_{½}$ values (in μM) were higher in the presence of 1 mM $MgCl_2$, 587 ± 337 for GDP and 727 ± 251 for GTP (Table 2). $K_{½}$ for ATP in the absence of $MgCl_2$ was 756 ± 232 μM (supplemental Fig. S4, *G* and *H*). Thus, the nucleotide affinity rank-order profile for Rv1739c STAS appeared to be GDP > GTP > ATP. Maximum STAS fluorescence quench was observed at ≤400 μM nucleotide except in the case of ATP, which required 2 mM nucleotide. The percent quench varied from 19 (for GTP) and 49% for GDP (Table 2). These data suggest a nucleotide interaction surface in Rv1739C STAS that directly or indirectly perturbs Trp^{50} and/or the three Tyr residues through conformational effects on adjacent or interposed residues.

GTPase Activity Associated with Rv1739c STAS

Intrinsic signaling or enzymatic activities of bacterial SulP-associated STAS domains remain undefined. *B. subtilis* SpoIIAA exhibits GTPase activity (22), but the GTP-binding protein YtvA lacks detectable GTPase activity (48). We therefore evaluated Rv1739c for the presence of intrinsic nucleotidase activity. As shown in supplemental Fig. S5*A*, the FPLC-purified Rv1739c STAS preparation exhibited modest GTPase activity that was STAS-dependent, temperature-sensitive, inactivated by SDS (supplemental Fig. S5*B*), and time-dependent. STAS-associated ATPase activity was not detected (not shown).

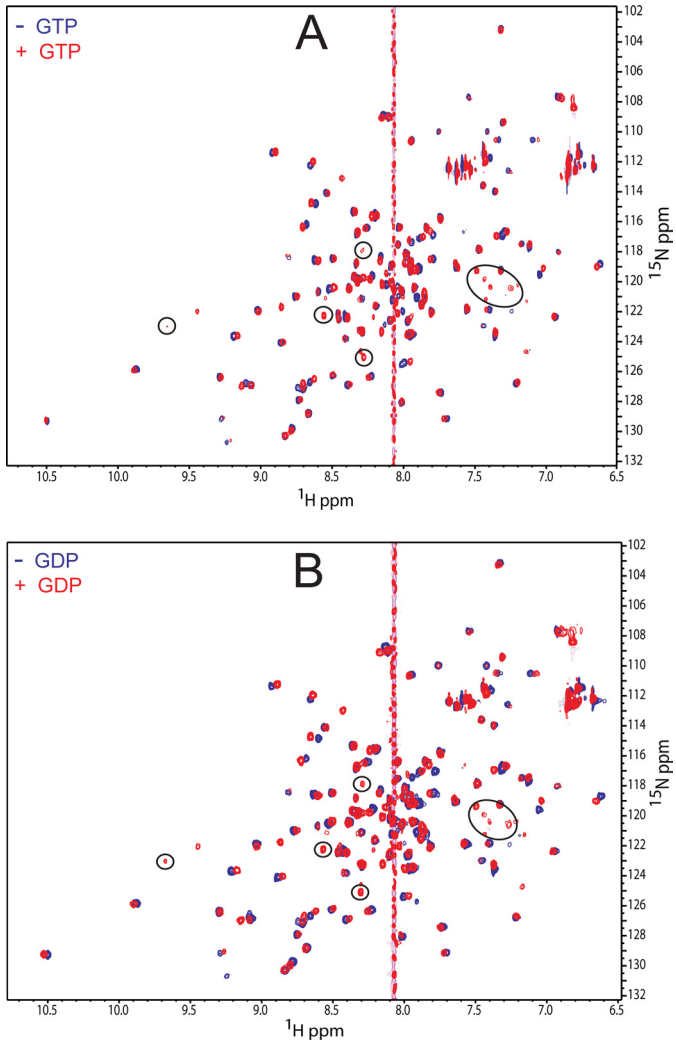

FIGURE 5. **NMR detection of guanine nucleotide interactions with Rv1739 STAS.** *A*, two-dimensional ^{1}H-^{15}N HSQC spectra of Rv1739c STAS in the absence (*blue contours*) and presence of 20 mM GTP (*red contours*). *B*, two-dimensional ^{1}H-^{15}N HSQC spectra of Rv1739c STAS in the absence (*blue contours*) and presence of 20 mM GDP (*red contours*). *Circled* resonances indicate residues detected only in the presence of nucleotide. The guanine proton peak is at ~8.07 ppm.

Residues Influenced by Nucleotide Binding in Rv1739c STAS

Fig. 5 shows two-dimensional ^{1}H-^{15}N HSQC overlays of Rv1739c STAS domain resonances in the absence (*blue* contours) and presence (*red* contours) of saturating concentrations of GTP (*A*) or GDP (*B*). Perturbations with weighted CSPs ($\Delta\delta_{weighted}$) ≥ 0.05 were considered significant (supplemental Fig. S6). CSP analysis revealed that the GDP-induced conformational change in Rv1739c STAS (Fig. 5*B*) affected a larger number of residues with greater extent of perturbation than those altered by the addition of GTP (Fig. 5*A*). GDP significantly perturbed 16 residues (*red* in Fig. 6, *C* and *D*), including Ala^{10}, Arg^{12}, Val^{13}, Gly^{15}, Val^{41}, Asp^{44}, Gln^{47}, Val^{48}, Arg^{79}, Gly^{106}, Glu^{107}, Asp^{108}, His^{109}, Ile^{110}, Arg^{122}, and Arg^{124}. GTP perturbed a subset of these residues (*red* in Fig. 6, *A* and *B*), including Ala^{10}, Arg^{12}, Val^{13}, Gly^{15}, Val^{48}, Val^{61}, Arg^{79}, His^{109}, and Arg^{124}. The results are consistent with the lower $K_{½}$ value for GDP than for GTP (Fig. 4 and Table 2). The amino acids exhibiting the largest GDP-induced CSPs are

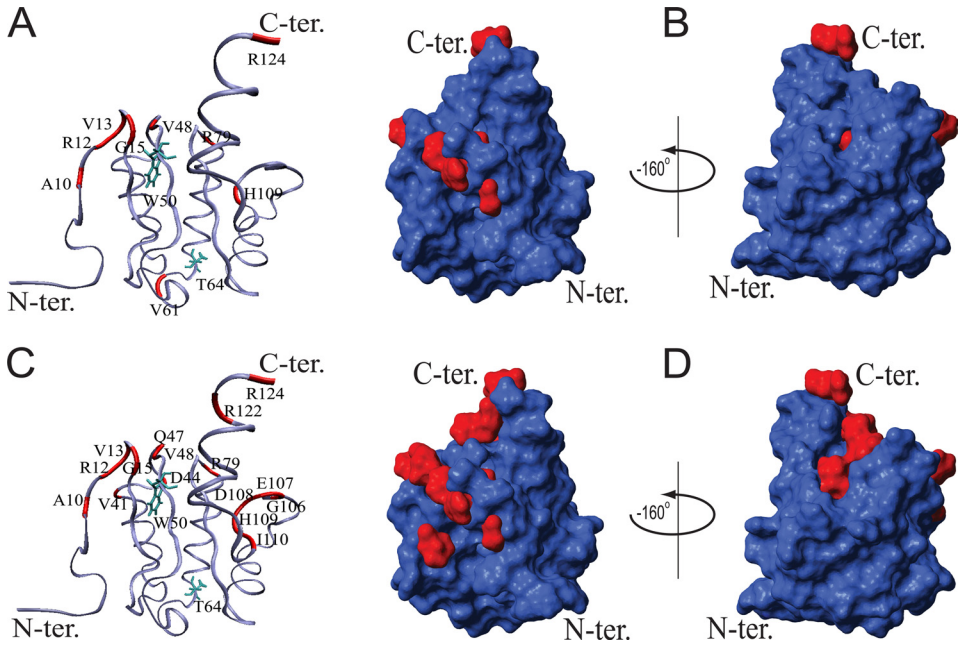

FIGURE 6. **Guanine nucleotide-shifted residues highlighted in the Rv1739c STAS structure.** *A* and *C*, STAS backbone representation is in *blue*; residues perturbed by ≥0.05 ppm following addition of 20 mM GTP (*A*) or GDP (*C*) are in *red*. *B* and *D*, the van der Waal surface representation of STAS structure (shown in two orientations) is in *blue*; residues were perturbed by ≥0.05 ppm following addition of 20 mM GTP (*B*) or GDP (*D*) are in *red* and annotated. Side chains of annotated residues Trp^{50} and Thr^{64} are in *cyan*.

illustrated at higher resolution in supplemental Fig. S6, *A* and *B*.

The observed nucleotide-induced conformational perturbations were predominantly localized within the solvent-exposed loops and immediately adjacent residues, as evidenced by the conformational flux of Val^{41} at the end of helix α_1, of Ile^{110} localized at the end of strand β_4, and Arg^{122} near the end of the C-terminal helix α_5. Many nucleotide-perturbed residues localize to a single face of Rv1739c STAS. Val^{61}, located near the semi-conserved, potential hydrolase nucleophile Thr^{64}, is the only residue perturbed >0.05 ppm by GTP alone (Fig. 6*A* and supplemental Fig. S6*C*).

Addition of GTP or GDP to Rv1739c resulted in emergence in the ^{1}H-^{15}N two-dimensional HSQC spectra of additional resonances (*circled* in Fig. 5, *A* and *B*) of near-identical (^{1}H, ^{15}N) coordinates. Line widths were broadened to a greater degree by GDP than by GTP. These ligand-induced resonances may belong to previously unassigned loop residues and/or to Ser^{95} in helix α3 (30). Alternatively, these resonances may reflect slow conformational exchange of select residues.

In Silico Docking of the STAS-Nucleotide Complex

Docking of GDP and GTP into the three-dimensional structure of Rv1739c STAS was performed using AutoDock Vina (44). These *in silico* experiments identified two potential nucleotide binding sites in Rv1739c STAS (supplemental Fig. S7). One site involves residues localized primarily near the STAS N terminus, whereas the other includes predominantly C-terminal residues.

STAS-GDP Docking—A flexible grid-based GDP-STAS docking protocol defined 9 clustered poses for the STAS domain bound to GDP, as illustrated under supplemental Fig. S7. In the lowest energy pose, the GDP-interacting amino acid residues include Gln^{9}, Gly^{15}, Tyr^{19}, Leu^{77}, Arg^{78}, Arg^{79}, Gly^{80}, Lys^{104}, Ile^{105}, Glu^{107}, Asp^{108}, Pro^{115}, Val^{118}, Gln^{119}, and Arg^{122}. Many of these residues are, or are adjacent to, those exhibiting above-threshold CSP in NMR titration studies. GDP binding is preferentially clustered to C-terminal STAS residues, with 7/9 poses supporting this preferred docked complex.

STAS-GTP Docking—Several interacting amino acids identified in the STAS-GDP complex were also identified in the GTP-STAS complex. However, GTP exhibited a modest preference for the STAS N terminus over its C terminus. The GTP-interacting residues of the clustered poses included Gln^{9}, Gly^{15}, Leu^{77}, Arg^{78}, Arg^{79}, Gly^{80}, Lys^{104}, Ile^{105}, Glu^{107}, Asp^{108}, Val^{118}, Gln^{119}, and Arg^{122} (supplemental Fig. S7).

Rv1739c STAS Appears Not to Be a Phosphoprotein

Mass spectrometric analysis of the Rv1739c STAS domain isolated from *E. coli* revealed no phosphate. Because the Rv1739c STAS polypeptide may have undergone dephosphorylation during purification, we evaluated its ability to serve as an *in vitro* phosphorylation substrate. Supplemental Fig. S8 shows, however, that none of the 11 recombinant, purified *M. tuberculosis* Ser/Thr kinases stably phosphorylated the Rv1739c STAS domain *in vitro*. Moreover, Rv1739c STAS did not serve as the phosphorylation substrate for any of the four purified, recombinant *M. tuberculosis* anti-σ factors.

Given that the isolated Rv1739c STAS may be a poor phosphorylation substrate *in vitro*, we assessed the phosphorylation status of FLAG-tagged Rv1739c STAS overexpressed in *M. smegmatis*. Importantly the Rv1739c overexpressed in *M. smegmatis* lacked an immunodetectable phosphothreonine

(not shown), further supporting the conclusion that Rv1739c is not a substrate for mycobacterial Ser/Thr or anti-σ factor kinases.

DISCUSSION

We have reported the three-dimensional NMR structure of the STAS domain from the SulP/SLC26 polypeptide Rv1739c of *M. tuberculosis*. We have compared this structure with previously solved structures of anti-σ factor antagonists, as well as with structures of STAS domain structures from putative anion transporters reported during review of this manuscript. Rv1739c STAS exhibited binding of nucleotides with affinities at the upper end of the physiological range, and with rank order of GDP > GTP ≫ ATP. GDP and GTP elicited distinct conformational changes in the Rv1739c STAS structure. Low rates of GTP hydrolysis were associated with nominally pure Rv1739c STAS. Rv1739c STAS underwent no detectable phosphorylation *in vitro*, or when overexpressed in *E. coli* or *M. smegmatis*.

Solution Structure of Rv1739c STAS—Despite its very limited amino acid sequence similarity to other STAS domains, the Rv1739c STAS solution structure superimposes closely with previously reported NMR and x-ray crystallography structures of anti-σ factor antagonists. However, in its absence of a β strand within the most N-terminal residues 1–14, Rv1739c STAS differs from the structured N-terminal regions observed in the other anti-σ factor antagonist structures (see above). The lack of N-terminal structure may be intrinsic to Rv1739c STAS, perhaps due in part to the presence of two proline residues: Pro^{8} and Pro^{14}, which may contribute to the conformational heterogeneity and general disruption of short β strand formation in this region. Alternatively, the lack of N-terminal structure may reflect the absence of particular additional residues in this construct (*i.e.* ~420–426) that link the reported STAS domain structure to the C-terminal end of the transmembrane domain, or the absence of a physiological interacting protein or ligand. With the exception of this unstructured N-terminal region, the Rv1739c backbone is a well defined, rigid/ordered structure, as shown by heteronuclear NOE data (supplemental Fig. S3*B*). The short intervening loop connecting regions of the secondary structure in Rv1739c resemble those of other anti-σ factor antagonists and *E. coli* SulP ychM (18), but contrast with the longer intervening loops in STAS domains of mammalian SLC26 proteins (Fig. 3, *D* and *E*).

The Rv1739c STAS domain construct studied here lacks the 15-aa N-terminal extension present in the crystal structure of the C-terminal truncated, IVS-deleted rat prestin STAS structure (Fig. 3*E*). This 15-aa extension includes the first β-strand ("β1") observed in rat prestin STAS (31). Deletion from the prestin STAS domain of its 73-aa IVS, of yet unknown function, was crucial for its crystallization, as was truncation from the rat prestin construct of its C-terminal 9 aa (31). Indeed, the secondary structure prediction program Psipred also predicts the presence of this β1 strand in rat prestin STAS containing the IVS, but considerably shortened compared with β1 in the crystal structure. Moreover, Psipred predicts the presence of the β1 strand in all human SLC26 STAS domains modified to include comparable IVS deletions. However, without computational deletion of this IVS, only SLC26A1, SLC26A2, and SLC26A7 are predicted to retain the β1 strand, whereas SLC26A3, SLC26A4, SLC26A6, SLC26A8, SLC26A9, and SLC26A11 are predicted to lack the β1 strand.

In contrast, the secondary structure prediction program Yaspin suggests that the presence of this STAS β1 strand of prestin is IVS-independent in rat prestin and in some other human SLC26 polypeptide paralogs. However, Yaspin also predicts the absence of the β1 strand structure from the STAS domains of human SLC26A1, SLC26A3, SLC26A4, and SLC26A11, as well as from the STAS domains of *Arabidopsis thaliana* sulfate transporters Sultr2.1 and Sultr2.2. Thus, the β1 strand may not be an essential part of all STAS domain structures, and its presence in some *SLC26* gene products may be influenced by the presence or absence of the IVS sequence.

Residues Pro^{543}, Tyr^{545}, Tyr^{546}, and Val^{655} of the rat prestin STAS domain have been proposed to constitute a juxtamembrane binding surface. The corresponding Rv1739c STAS residues Pro^{24}, Cys^{26}, Phe^{27}, and Thr^{64} are similarly oriented. Such an interaction could be with the lipid bilayer or, as proposed for *Synechococcus* BicA, with a cytoplasmic loop of the SulP transmembrane domain.

Rv1739c STAS Is a Nucleotide-binding Protein—Photoactivated 8-N_3-biotinyl-GTP labeled Rv1739c STAS, and labeling was blocked in the presence of excess GTP (Fig. 4*A*). We monitored the intrinsic fluorescence of Rv1739c STAS as a function of added nucleotide rather than directly monitoring fluorophor-labeled nucleotides, because these latter experiments often exhibit unique, fluorophor-related changes in ligand binding affinity and/or hydrolytic activity that are specific to individual GTP-binding proteins (49). Both GTP and GDP quenched the intrinsic fluorescence of Rv1739c STAS (Fig. 4), consistent with nucleotide binding directly or indirectly altering the electrostatic environments of residues Trp^{50} and/or Tyr^{7}, Tyr^{19}, or Tyr^{21}. The $K_{½}$ for GDP binding was 146 μM, about half the value for GTP. $K_{½}$ values for both GDP and GTP were indistinguishable from those of their respective thioester analogs. The $K_{½}$ for binding of ATP was ~2-fold higher than for GTP (supplemental Fig. S4*F*), a property shared with SpoIIAA (22). The presence of 1 mM Mg^{2+} reduced binding affinity 2-fold for GTP and ~4-fold for GDP (Table 2), as noted for the STAS domain of *B. subtilis* photosensor YtvA (48). These data are the first to demonstrate guanine nucleotide binding to a SulP transporter STAS domain. The low guanine nucleotide binding affinities of Rv1739c STAS are within the range of previously reported GTP binding constants as high as 1.1 mM (supplemental Table S1), but contrast with the GTP $K_{½}$ of 0.25 μM reported for *B. subtilis* SpoIIAA (22).

Rv1739c STAS Nucleotide Binding Site(s)—NMR CSP studies (Fig. 5 and supplemental Fig. S6) suggest a semi-contiguous surface in Rv1739c STAS involved in binding GDP and/or GTP (Fig. 6). Among the Rv1739c STAS residues perturbed by >0.05 ppm in the presence of nucleotides, Val^{41} and Val^{61} (and Val^{48} to a lesser degree) are hydrophobic residues conserved in other anti-σ factor antagonists and in STAS domains (Fig. 3*D*). *In silico* docking of STAS with GDP and GTP (supplemental Fig. S7) supported involvement of residues per-

turbed in the CSP studies (Figs. 5 and 6, and supplemental Fig. S6). Similar to the NMR CSP data, 7 of the 9 calculated poses in the presence of GDP support binding to an interface that involves residues localized within the C-terminal region of the STAS domain, including aa Gly^{106}–Ile^{110} (Fig. 6*C* and supplemental S6*D*). The CSP data suggest (with support from the docked poses) that the C-terminal binding site is perturbed to a greater degree by GDP than by GTP (Figs. 5 and 6, and supplemental Fig. S6, *C* and *D*). GTP docking involved only a subset of residues at this interface, as well as additional residues of the STAS N-terminal region (supplemental Fig. S7*A*). Some of the nucleotide-perturbed residues, including those of the N-terminal region, Val^{48} and Val^{61}, correspond to regions in anti-σ factor antagonist TM1081, which exhibit millisecond scale conformational changes in solution but not in the crystal, suggesting their involvement in binding or catalytic activity (27).

The CSP data and docking calculations suggest two possible nucleotide binding sites in the presence of 20 mM nucleotide, whereas intrinsic fluorescence quench data at 30–100-fold lower nucleotide concentrations are compatible with a single binding site (Table 2). The single binding site predicted from fluorescence quench measurements may be one of the two sites suggested by CSP and docking calculations, with recruitment of the second site only at much higher ligand concentrations. Alternatively, both sites may bind nucleotide in the physiological concentration range, with only one of the sites influencing intrinsic fluorescence. The positioning of the Tyr and Trp residues in Rv1739c STAS suggests the N-terminal site could be that site.

GTPase Activity Associated with Rv1739c STAS—Anti-σ factor antagonists differ in their nucleotide hydrolase activities. Whereas SpoIIAA hydrolyzed GTP (22), YtvA had undetectable GTP hydrolase activity (47, 50). Rv1739c STAS-associated GTPase activity was detectable as slow inorganic [^{32}P]phosphate release from [γ-^{32}P]GTP (supplemental Fig. S5) in the nominal absence of Mg^{2+}. The hydrolysis rate was not increased upon addition of 1 mM Mg^{2+}. Rv1739c STAS-associated GTPase activity was only ~8-fold lower than that of RhoA-GST in the same conditions. The low rates thus likely reflect low input substrate concentrations, because measured Rv1739c STAS GTPase activity was orders of magnitude slower than that reported for SpoIIAA in the presence of the ratio $[GTP]/K_{½(GTP)} = 30$ (22). However, Rv1739c STAS-associated subsaturated GTPase activity was only ~20–50-fold lower than the GTP-saturated GTPase rates of *Saccharomyces cerevisiae* Ypt6 (51, 52) and human Rheb (49). Thus, Rv1739c STAS-associated GTPase activity was near the low-end of the reported GTPase rates. Nonetheless, the presence of copurifying contaminant GTPase(s) in our Rv1739c STAS preparation remains a potential explanation.

Possible Physiological Roles of GTP Binding by Rv1739c STAS—The GTP $K_{½}$ value within the intracellular range of [GTP] suggests a physiological role for nucleotide binding by Rv1739c STAS. Nucleotide binding might regulate Rv1739c localization or anion transport that is mediated by or associated with Rv1739c function, directly or through alteration of protein-protein interaction.

Rv1739c STAS, unlike SpoIIAA, was not detectably phosphorylated (supplemental Fig. S8). The mechanistic role of SpoIIAA phosphorylation remains unclear, because substitution of this serine residue by acidic residues did not phenocopy the activity of serine phosphorylation (24, 25, 27). The STAS domains of human SLC26A3 (29) and human SLC26A9 (53) interact *in vitro* with the phosphorylated R domain of CFTR, but the reported regulatory interactions of SLC26 polypeptides and CFTR *in vitro* and *in vivo* have varied. PKC phosphorylation of the human SLC26A6 STAS domain has been suggested to regulate Cl^-/HCO_3^- exchange activity through CAII binding (54), but this phosphorylation did not regulate oxalate transport (55), and its relationship to CFTR is unknown. Although the R domain of CFTR is not shared among other ABC proteins, Rv1739c might function as a regulator of the *M. tuberculosis* ABC family sulfate permease CysTWA (15). *E. coli* ychM STAS domain has been shown to interact with subunits of other ABC family permeases (18).

M. bovis cysA mutants lack sulfate uptake in resting cultures (56), yet *cysA* and *subI* sulfate uptake mutants of *Mycobacterium bovis* survive in mice as well as wild type *M. bovis* (57). Thus, under the stressful conditions inside acidifying compartments of cells, mycobacteria might rely on stress-regulated expression of SulP Rv1739c. Indeed, Rv1739c is among the sulfate transport and metabolism genes up-regulated in the dormant phase of infection in cultured macrophages and in granulomas of intact mice (58). Similarly, the STAS domain-containing SulP protein ychM of *E. coli* is also up-regulated in stress conditions of RpoN (σ54) deletion (59) and nitrofurantoin treatment (60), and severely down-regulated in a virulence-impaired *E. coli* O157:H7 strain with deletion of the conserved, alternative σ factor and stress regulator RpoS (61). The recent discoveries that *E. coli* ychM binds to acyl carrier protein, an abundant, small polypeptide with many additional interaction partners (62), and that its deletion influences multiple gene products that regulate fatty acid biosynthesis (18), add new complexity to these questions. Furthermore, stress regulation (as nutrient supply and redox potential) has been proposed to regulate, on a cyclical basis, the direct interaction of *A. thaliana* SulP sulfate transporter Sultr1;2 with the cysteine synthase, *O*-acetylserine (thiol) lyase (63). A STAS-related or STAS-mediated guanine nucleotide cycle could potentially regulate the proposed cycle of binding and unbinding. Thus, the STAS domain of SulP anion transporters may sense environmental or metabolic stress through nucleotide binding, exchange, and/or hydrolysis to modulate anion transport and/or scaffolding of signaling proteins or enzymes as part of the regulation of cell metabolism and other functions.

Acknowledgments—We thank Dr. John F. Heneghan (Beth Israel Deaconess Medical Center) and Drs. James Sudmeier and Gillian Henry (Tufts University Biological NMR Center) for helpful discussion. All NMR experiments were performed at the Tufts University Biological NMR Center.

REFERENCES

1. Sherman, T., Chernova, M. N., Clark, J. S., Jiang, L., Alper, S. L., and Nehrke, K. (2005) *Am. J. Physiol. Cell Physiol.* **289,** C341–C351

2. Felce, J., and Saier, M. H., Jr. (2004) *J. Mol. Microbiol. Biotechnol.* **8,** 169–176
3. Dorwart, M. R., Shcheynikov, N., Yang, D., and Muallem, S. (2008) *Physiology* **23,** 104–114
4. Hästbacka, J., de la Chapelle, A., Mahtani, M. M., Clines, G., Reeve-Daly, M. P., Daly, M., Hamilton, B. A., Kusumi, K., Trivedi, B., and Weaver, A. (1994) *Cell* **78,** 1073–1087
5. Höglund, P., Haila, S., Socha, J., Tomaszewski, L., Saarialho-Kere, U., Karjalainen-Lindsberg, M. L., Airola, K., Holmberg, C., de la Chapelle, A., and Kere, J. (1996) *Nat. Genet.* **14,** 316–319
6. Everett, L. A., Glaser, B., Beck, J. C., Idol, J. R., Buchs, A., Heyman, M., Adawi, F., Hazani, E., Nassir, E., Baxevanis, A. D., Sheffield, V. C., and Green, E. D. (1997) *Nat. Genet.* **17,** 411–422
7. Liu, X. Z., Ouyang, X. M., Xia, X. J., Zheng, J., Pandya, A., Li, F., Du, L. L., Welch, K. O., Petit, C., Smith, R. J., Webb, B. T., Yan, D., Arnos, K. S., Corey, D., Dallos, P., Nance, W. E., and Chen, Z. Y. (2003) *Hum. Mol. Genet.* **12,** 1155–1162
8. Jiang, Z., Asplin, J. R., Evan, A. P., Rajendran, V. M., Velazquez, H., Nottoli, T. P., Binder, H. J., and Aronson, P. S. (2006) *Nat. Genet.* **38,** 474–478
9. Dawson, P. A., Russell, C. S., Lee, S., McLeay, S. C., van Dongen, J. M., Cowley, D. M., Clarke, L. A., and Markovich, D. (2010) *J. Clin. Invest.* **120,** 706–712
10. Xu, J., Song, P., Nakamura, S., Miller, M., Barone, S., Alper, S. L., Riederer, B., Bonhagen, J., Arend, L. J., Amlal, H., Seidler, U., and Soleimani, M. (2009) *J. Biol. Chem.* **284,** 29470–29479
11. Xu, J., Song, P., Miller, M. L., Borgese, F., Barone, S., Riederer, B., Wang, Z., Alper, S. L., Forte, J. G., Shull, G. E., Ehrenfeld, J., Seidler, U., and Soleimani, M. (2008) *Proc. Natl. Acad. Sci. U.S.A.* **105,** 17955–17960
12. Tuo, B., Riederer, B., Wang, Z., Colledge, W. H., Soleimani, M., and Seidler, U. (2006) *Gastroenterology* **130,** 349–358
13. Wang, Y., Soyombo, A. A., Shcheynikov, N., Zeng, W., Dorwart, M., Marino, C. R., Thomas, P. J., and Muallem, S. (2006) *EMBO J.* **25,** 5049–5057
14. Ishiguro, H., Namkung, W., Yamamoto, A., Wang, Z., Worrell, R. T., Xu, J., Lee, M. G., and Soleimani, M. (2007) *Am. J. Physiol. Gastrointest. Liver Physiol.* **292,** G447–455
15. Zolotarev, A. S., Unnikrishnan, M., Shmukler, B. E., Clark, J. S., Vandorpe, D. H., Grigorieff, N., Rubin, E. J., and Alper, S. L. (2008) *Comp. Biochem. Physiol. A Mol. Integr. Physiol.* **149,** 255–266
16. Price, G. D., Woodger, F. J., Badger, M. R., Howitt, S. M., and Tucker, L. (2004) *Proc. Natl. Acad. Sci. U.S.A.* **101,** 18228–18233
17. Shelden, M. C., Howitt, S. M., and Price, G. D. (2010) *Mol. Membr. Biol.* **27,** 12–23
18. Babu, M., Greenblatt, J. F., Emili, A., Strynadka, N. C., Reithmeier, R. A., and Moraes, T. F. (2010) *Structure* **18,** 1450–1462
19. Aravind, L., and Koonin, E. V. (2000) *Curr. Biol.* **10,** R53–55
20. Clarkson, J., Campbell, I. D., and Yudkin, M. D. (2003) *Biochem. J.* **372,** 113–119
21. Masuda, S., Murakami, K. S., Wang, S., Anders Olson, C., Donigian, J., Leon, F., Darst, S. A., and Campbell, E. A. (2004) *J. Mol. Biol.* **340,** 941–956
22. Najafi, S. M., Harris, D. A., and Yudkin, M. D. (1996) *J. Bacteriol.* **178,** 6632–6634
23. Kuo, S., Demeler, B., and Haldenwang, W. G. (2008) *J. Bacteriol.* **190,** 6625–6635
24. Kovacs, H., Comfort, D., Lord, M., Campbell, I. D., and Yudkin, M. D. (1998) *Proc. Natl. Acad. Sci. U.S.A.* **95,** 5067–5071
25. Seavers, P. R., Lewis, R. J., Brannigan, J. A., Verschueren, K. H., Murshudov, G. N., and Wilkinson, A. J. (2001) *Structure* **9,** 605–614
26. Etezady-Esfarjani, T., Placzek, W. J., Herrmann, T., and Wüthrich, K. (2006) *Magn. Reson. Chem.* **44,** S61–70
27. Serrano, P., Pedrini, B., Geralt, M., Jaudzems, K., Mohanty, B., Horst, R., Herrmann, T., Elsliger, M. A., Wilson, I. A., and Wüthrich, K. (2010) *Acta Crystallogr. Sect. F Struct. Biol. Cryst. Commun.* **66,** 1393–1405
28. Quin, M., Newman, J., Firbank, S., Lewis, R. J., and Marles-Wright, J. (2008) *Acta Crystallogr. Sect. F Struct. Biol. Cryst. Commun.* **64,** 196–199
29. Dorwart, M. R., Shcheynikov, N., Baker, J. M., Forman-Kay, J. D., Muallem, S., and Thomas, P. J. (2008) *J. Biol. Chem.* **283,** 8711–8722
30. Sharma, A. K., Ye, L., Zolotarev, A. S., Alper, S. L., and Rigby, A. C. (2009) *Biomol. NMR Assign.* **3,** 99–102
31. Pasqualetto, E., Aiello, R., Gesiot, L., Bonetto, G., Bellanda, M., and Battistutta, R. (2010) *J. Mol. Biol.* **400,** 448–462
32. Delaglio, F., Grzesiek, S., Vuister, G. W., Zhu, G., Pfeifer, J., and Bax, A. (1995) *J. Biomol. NMR* **6,** 277–293
33. Kraulis, P. J., Domaille, P. J., Campbell-Burk, S. L., Van Aken, T., and Laue, E. D. (1994) *Biochemistry* **33,** 3515–3531
34. Cavanagh, J., Fairbrother, W. J., Palmer, A. G., and Skelton, N. J. (1996) *Protein NMR Spectroscopy: Principles and Practice*, Academic Press Inc., San Diego, CA
35. Bax, A., and Grzesiek, S. (1993) *Acc. Chem. Res.* **26,** 131–138
36. Muhandiram, D. R., Farrow, N. A., Xu, G. Y., Smallcombe, S., and Kay, L. E. (1993) *J. Magn. Reson. Ser. B* **102,** 317–321
37. Güntert, P., Mumenthaler, C., and Wüthrich, K. (1997) *J. Mol. Biol.* **273,** 283–298
38. Cornilescu, G., Delaglio, F., and Bax, A. (1999) *J. Biomol. NMR* **13,** 289–302
39. Sharma, A. K., Sharma, S. K., Surolia, A., Surolia, N., and Sarma, S. P. (2006) *Biochemistry* **45,** 6904–6916
40. Linge, J. P., Williams, M. A., Spronk, C. A., Bonvin, A. M., and Nilges, M. (2003) *Proteins* **50,** 496–506
41. Laskowski, R. A., Rullmannn, J. A., MacArthur, M. W., Kaptein, R., and Thornton, J. M. (1996) *J. Biomol. NMR* **8,** 477–486
42. Koradi, R., Billeter, M., and Wuthrich, K. (1996) *J. Mol. Graph.* **14,** 51–55, 29–32
43. Humphrey, W., Dalke, A., and Schulten, K. (1996) *J. Mol. Graph.* **14,** 33–38, 27–28
44. Trott, O., and Olson, A. J. (2010) *J. Comput. Chem.* **31,** 455–461
45. Rao, A., Martin, P., Reithmeier, R. A., and Cantley, L. C. (1979) *Biochemistry* **18,** 4505–4516
46. Greenstein, A. E., MacGurn, J. A., Baer, C. E., Falick, A. M., Cox, J. S., and Alber, T. (2007) *PLoS Pathog.* **3,** e49
47. Buttani, V., Losi, A., Polverini, E., and Gärtner, W. (2006) *FEBS Lett.* **580,** 3818–3822
48. Tang, Y., Cao, Z., Livoti, E., Krauss, U., Jaeger, K. E., Gärtner, W., and Losi, A. (2010) *Photochem. Photobiol. Sci.* **9,** 47–56
49. Mazhab-Jafari, M. T., Marshall, C. B., Smith, M., Gasmi-Seabrook, G. M., Stambolic, V., Rottapel, R., Neel, B. G., and Ikura, M. (2010) *J. Biol. Chem.* **285,** 5132–5136
50. Avila-Pérez, M., Vreede, J., Tang, Y., Bende, O., Losi, A., Gärtner, W., and Hellingwerf, K. (2009) *J. Biol. Chem.* **284,** 24958–24964
51. Bergbrede, T., Chuky, N., Schoebel, S., Blankenfeldt, W., Geyer, M., Fuchs, E., Goody, R. S., Barr, F., and Alexandrov, K. (2009) *J. Biol. Chem.* **284,** 2628–2635
52. Bergbrede, T., Pylypenko, O., Rak, A., and Alexandrov, K. (2005) *J. Struct. Biol.* **152,** 235–238
53. Chang, M. H., Plata, C., Sindic, A., Ranatunga, W. K., Chen, A. P., Zandi-Nejad, K., Chan, K. W., Thompson, J., Mount, D. B., and Romero, M. F. (2009) *J. Biol. Chem.* **284,** 28306–28318
54. Alvarez, B. V., Vilas, G. L., and Casey, J. R. (2005) *EMBO J.* **24,** 2499–2511
55. Hassan, H. A., Mentone, S., Karniski, L. P., Rajendran, V. M., and Aronson, P. S. (2007) *Am. J. Physiol. Cell Physiol.* **292,** C1485–1492
56. Wooff, E., Michell, S. L., Gordon, S. V., Chambers, M. A., Bardarov, S., Jacobs, W. R., Jr., Hewinson, R. G., and Wheeler, P. R. (2002) *Mol. Microbiol* **43,** 653–663
57. Niederweis, M. (2008) *Microbiology* **154,** 679–692
58. Murphy, D. J., and Brown, J. R. (2007) *BMC Infect. Dis.* **7,** 84
59. Riordan, J. T., Tietjen, J. A., Walsh, C. W., Gustafson, J. E., and Whittam, T. S. (2010) *Microbiology* **156,** 719–730
60. Liu, A., Tran, L., Becket, E., Lee, K., Chinn, L., Park, E., Tran, K., and Miller, J. H. (2010) *Antimicrob. Agents Chemother.* **54,** 1393–1403
61. Dong, T., and Schellhorn, H. E. (2009) *BMC Genomics* **10,** 349
62. Byers, D. M., and Gong, H. (2007) *Biochem. Cell Biol.* **85,** 649–662
63. Shibagaki, N., and Grossman, A. R. (2010) *J. Biol. Chem.* **285,** 25094–25102